Self-applied Magnetic Field Intensity Effects on Solid Propellant Mpd Thruster Performance*

Luigi Petrucci and Giorgio Paccani
Università degli Studi di Roma "La Sapienza"
Dipartimento Meccanica e Aeronautica,
Via Eudossiana 18, 00184 Rome, Italy.
Rome Italy
+39.06.44585283
g.paccani@dma.ing.uniroma1.it

IEPC-01-139

The effect on solid propellant MPD thruster behavior of different axial self-applied magnetic fields was investigated. The thrusters have coaxial electrodes with six radially-mounted propellant bars surrounding the cathode. The self-applied magnetic fields were respectively generated by a six- and a twelve-turn coil. Measurements included electrical characteristics, impulse bit (thrust stand), exhaust velocity (TOF Langmuir probe system), and ablated propellant mass per shot. Under constant current, higher self-applied magnetic fields lead to higher impedances, higher ablated mass, and higher impulse bit. However at constant energy per shot, the impulse bit gained by applying the magnetic field does not justify the energy lost to feed the coil.

Nomenclature

MPD Magnetoplasmadynamic
PFN Pulse forming network
PVC Polyvinyl chloride
TOF Time of flight

Symbols

b Theoretical law coefficient, N/A^2
B Magnetic field, T
C Capacitance, C
E Energy, J
f Volume force, N/m^3
F Thrust, N
I_b Impulse bit, N s
i Current, A
J Current density, A/m^3
K i^2/m
m Ablated mass per shot, Kg
P Power, W
r Radius
t Time, s
V Potential, V
w Exhaust velocity, m/s
Z Impedance, Ω
η Efficiency
τ Discharge duration, s
Ψ Current Parameter, $\int i^2 \, dt$, A^2 s

Subscripts

Max Maximum
r Radial component
t Thrust
T Thruster
th Theoretical
z Axial component
θ Azimuthal component
0 Initial or set value

Introduction

This paper deals with the effects of self-applied magnetic field intensity on working and performance parameters of coaxial solid propellant MPD thrusters (Fig. 1) operating in pulsed mode with instantaneous power levels of a few megawatts during pulses (shots) which last approximately one millisecond. In these electromagnetic thrusters the propellant mass flow rate is not an externally controllable variable; performance is

determined by engine scale[1], arc and propellant properties[2,3,4], arc-propellant interaction[5,6] and engine geometry[7,8].

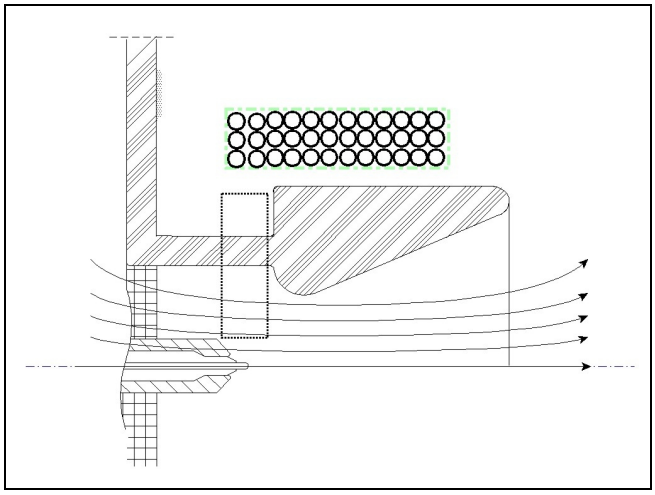

Figure 1 - MPD Discharge chamber with Self-applied magnetic field.

It is widely known that, in a stationary MPD thruster with self-induced magnetic field, the thrust is a function of the anode radius, r_a, and cathode radius, r_c, through the relation[9],

$$F = b\, i^2 \qquad (1)$$

where,

$$b = \ln\left(\frac{r_a}{r_c}\right) + \frac{3}{4} \quad . \qquad (2)$$

The parameter "b" is the electromagnetic thrust coefficient also called the Maecker law[10] coefficient. In a pulsed thruster, the relation becomes

$$I_b = b\, \Psi \qquad (3)$$

where,

$$\Psi = \int_0^{\tau} i^2\, dt\,. \qquad (4)$$

The Maecker law can be theoretically derived by a simplified bidimensional treatment and is in good agreement with experimental results[8].

The presence of an applied axial magnetic field, which is superimposed upon the self-induced one, modifies the phenomena inside the acceleration duct, and hence modifies the resulting thrust[11-15].

The interaction between this external magnetic field and the discharge causes a plasma swirling motion around the thruster axis. The phenomena inside the thruster, although still azimuthally symmetric, can no longer be treated as bi-dimensional phenomena.

In previous studies[16,17], the impact of a "self-applied" magnetic field generated by coaxial coils, on the behavior of coaxial ablative pulsed MPD thrusters has been examined, while varying the discharge chamber geometry, the anodic configuration, and the coils configuration and axial position. The effects of the magnetic field, due to a two-turn or six-turn coil crossed by the same current creating the discharge, became more important augmenting the discharge energy, i.e. augmenting the magnitude of the magnetic field itself.

In this paper, the effects - at equal energy - on the behavior of an ablative MPD thruster of the self-applied magnetic field intensity will be examined. The magnetic fields with different intensity were respectively generated by a six- and a twelve-turn coil of equal length and equally positioned with respect to the same discharge chamber-anode-nozzle. Both coils surrounded 7/9 of the acceleration duct length (starting from the cathode tip) (see Fig. 1).

Experimental Setup

Thruster System

The MPD propulsive system consists of PFN (Pulse Forming Network), transmission line, thruster (with or without coil), start-up circuit.

The baseline thruster configuration (MIRA) is shown in Fig. 2 and is described in detail in previous works[18,19]. It has a coaxial geometry with a conductive (aluminum-silicon-manganese-alloy) converging-diverging discharge chamber-anode-nozzle and a cylindrical-conical cathode (copper). Six Teflon® propellant bars pass radially through the wall of the nozzle and in a symmetrical arrangement surround the cathode tip. A trigger electrode (tungsten) protrudes from the cathode within which it is co-axially located.

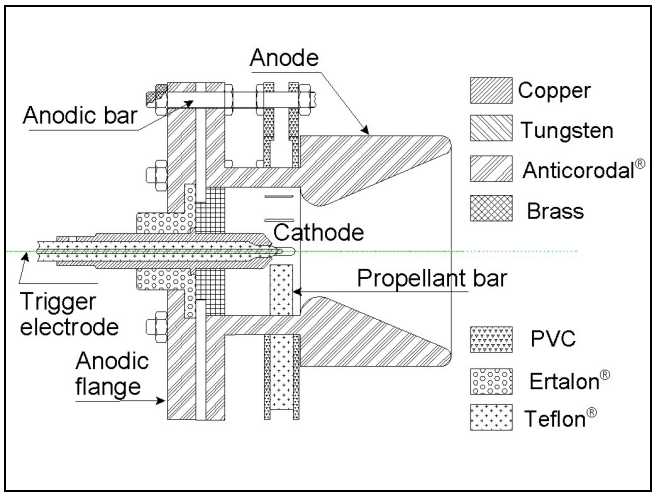

Figure 2 - Baseline MIRA solid propellant MPD thruster.

The two coils[19] (Fig. 3) have a length of 72 mm; this length was chosen in order to generate, inside the acceleration duct, an almost purely axial magnetic field (see Fig. 1). The coils consist of six copper cables - 2.5 mm^2 in section - wound around a cylinder of PVC. At the ends of the cylinder two 2.5 mm tick copper flanges are mounted. Six brass conductors connect the coil to the alimentation flange of the thruster ("in-going" conductors), while a further six connect it to the discharge chamber-anode-nozzle ("out-going" conductors). The winding of each of the six cables can be considered equivalent to six turns with a mean radius of 69 mm, or to twelve turns with a mean radius of 75 mm. In the followings, the MIRA thruster with the six-turn coil and the MIRA thruster with the twelve-turn coil are respectively denoted MIRA_L06 and MIRA_L12.

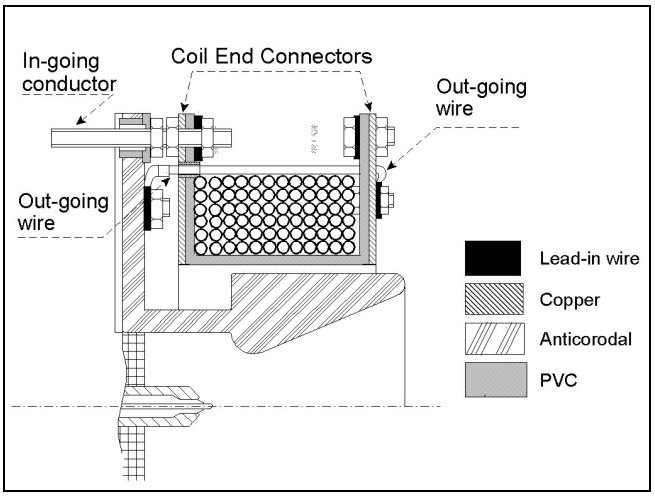

Figure 3 - A partial view of the twelve-turn coil mounted on the thruster.

The energy storage means consists of a capacitive Pulse Forming Network (PFN) with a total capacitance of 0.072 ± 0.002 F coaxially connected to the thruster electrodes. The PFN set voltage was the primary externally controllable variable during the tests.

Measurements and Procedures

Experimental measurements included the instantaneous electrical characteristics [PFN electrodes potential difference $V(t)$ and discharge current intensity $i(t)$], impulse bit (I_b), ion velocity in the exhaust jet (w), and ablated propellant mass per shot (m) for each thruster configuration. The PFN provided input energies, E_0, from 1333 J in increments of 333 J. Maximum energy value of 2333 and 3333 respectively were used for the MIRA_L12 and the other two thrusters.

The PFN output energy was defined by setting the PFN potential, V_0, according to

$$E_0 = \frac{1}{2} C V_0^2 . \qquad (5)$$

The electrode potential was measured by an oscilloscope while current was measured using a Rogowsky probe. A value averaged over 12 measurements was used as the standard value for each electrical parameter. The energy per shot

$$E_T = \int_0^{\infty} i(t) \cdot V(t)\, dt \qquad (6)$$

was computed using the measured electrical parameters.

The ablated propellant mass was obtained from the difference in weight of the propellant bars before and after each series of shots. The propellant bars were weighed using an electronic balance. The error in this measurement has been estimated to be a maximum of ±5 mg.

A thrust balance, described in detail elsewhere[20], was used to measure the thruster impulse bit based on an average value from 12 measurements.

Finally, the ion velocity in the exhaust was measured based on an average value from 30 TOF measurements obtained from cross correlation of the signals from two double Langmuir probes located downstream of the thruster[21].

Uncertainties were calculated using error propagation theory based on the standard deviation of the individual measurements.

The tests were conducted in a 0.5 m^3, polyvinyl chloride (PVC) vacuum tank with a nominal back pressure of 10^{-2} Pa. All of the instrumentation was housed in a full Faraday cage and data acquisition was computer-controlled.

Experimental Results

The electrical parameters of the different thrusters (with and without coil) differed greatly, leading to very different characteristic curves[19]: in Fig. 4 the current intensity, *i,* during an impulse, in each thruster, is shown as a function of the time at an input energy, E_0, of 2000 J. The presence of the coil lowers the maximum value, i_{Max}, of the current intensity while increasing the pulse duration. Augmenting the number of coils amplifies these effects. Moreover at an input energy, E_0, higher than 2333 J, the propulsive system with the 12-turns coil presents an "inversion" of the current (see Fig. 5), that can damage the capacitors. For this reason the thruster MIRA_L12 has not been tested with input energies higher than E_0=*2333*.

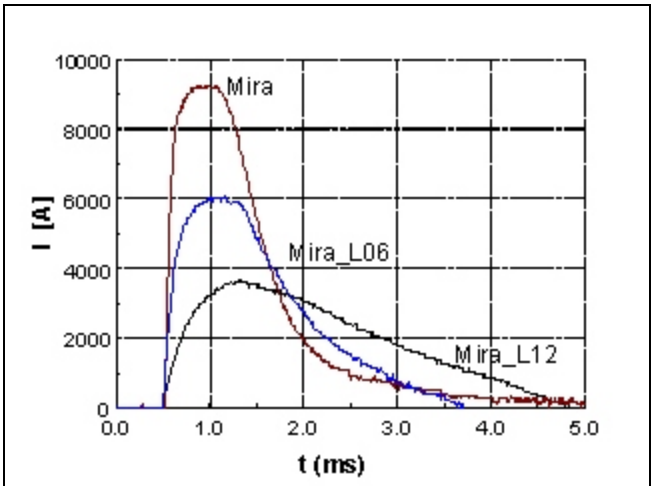

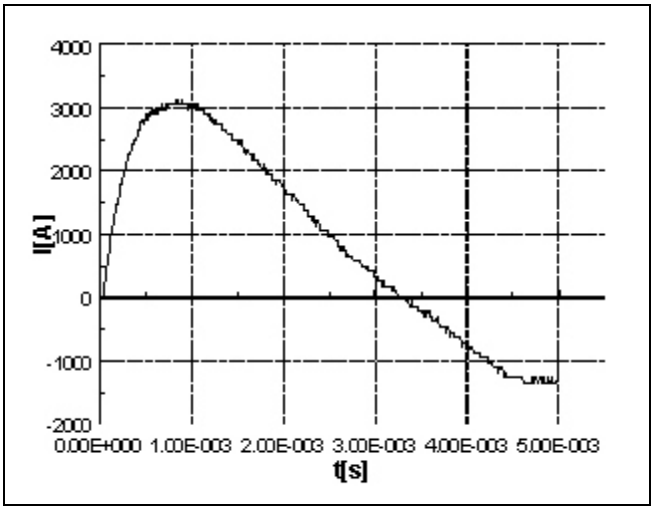

Figure 5 - Current versus time at input energy E_0 = *2666 J* for the MIRA_L12.

The differences between the characteristic curves of the three propulsive systems (PFN+transmission line+thruster), rend a comparison between the characteristic parameters of the different propulsive

systems at equal input energy, E_0, almost useless: the influence of the coupling is greater than any other effect.

Current parameter

To analyze the behavior of the thrusters thoroughly, the variation in the characteristic parameters with energy, E_T, and with the current parameter, Ψ, must be studied. Both of these parameters show linear increases as a function of input energy, E_0. When cross-plotting the energy E_T and current parameter (Fig. 6), the behavior is strictly linear. As expected, due to the coil impedance, this parameter has the highest values in the MIRA thruster and decreases while increasing the number of turns of the coil.

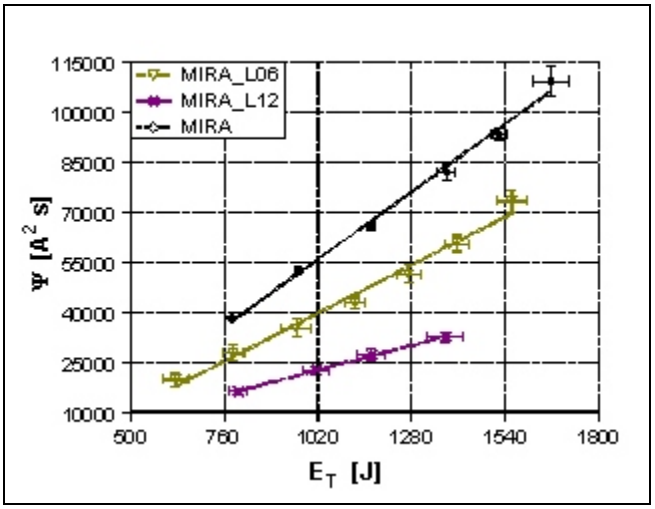

Figure 6 - Current parameter, Ψ, as a function of energy, E_T, shows a linear relationship.

The energy E_T accounts for the electrical losses in the transmission lines and in the thruster (coil, electrodes, discharge), while Ψ provides information on the only phenomena which occur into the discharge chamber regardless of electrical losses. In other words, graphs reported as a function of the thruster energy, E_T, account for the functioning of the thruster+transmission line system while the current parameter, Ψ, only account for the behavior of the acceleration duct. The results will be presented as a function of Ψ unless the use of E_T enables additional insights.

Impedance

The impedance of the (thruster+transmission line) system exhibits similar behavior both as function of E_T and Ψ, showing a parabolic decrease while tending towards a limiting constant value (see Fig. 7).

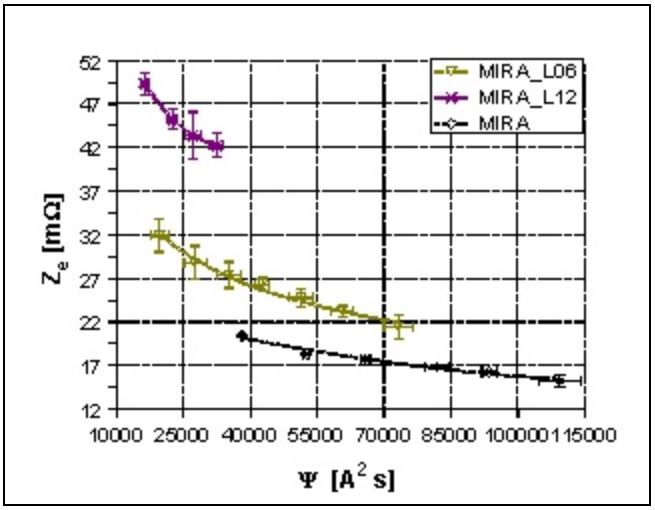

Figure 7 - Thruster system impedance, Z_e, versus current parameter, Ψ, shows the tendency towards a lower limiting constant value with increasing energy.

For constant E_T and Ψ, as can be expected from the presence of the coils, the impedance characteristics obey the following inequality:

$$\mathbf{Z_{MIRA\_L12} > Z_{MIRA\_L06} > Z_{MIRA}}.$$

Ablated mass

The ablated propellant mass per shot increases linearly with increasing energy, E_T, and current parameter, Ψ (see Fig. 8). At constant Ψ, both in terms of absolute values and slopes, the ablated mass characteristics obey the following inequality:

$$\mathbf{m_{MIRA\_L12} > m_{MIRA\_L06} > m_{MIRA}}\ .$$

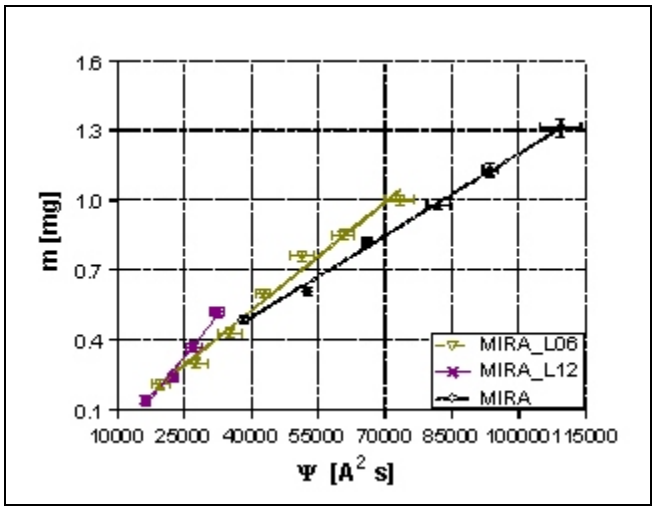

Figure 8 - The linear behavior of the ablated mass per shot, m, as a function of current parameter, Ψ.

K parameter

In the range of voltage over which the thruster exhibits its best behavior, the baseline MIRA shows a parameter

$$K = \frac{i^2}{\dot{m}} \qquad (7)$$

generally constant while exhibiting small irregularities, whilst the two thruster systems with the coil exhibit decreasing values, tending at a constant at the higher energies (Fig. 9).

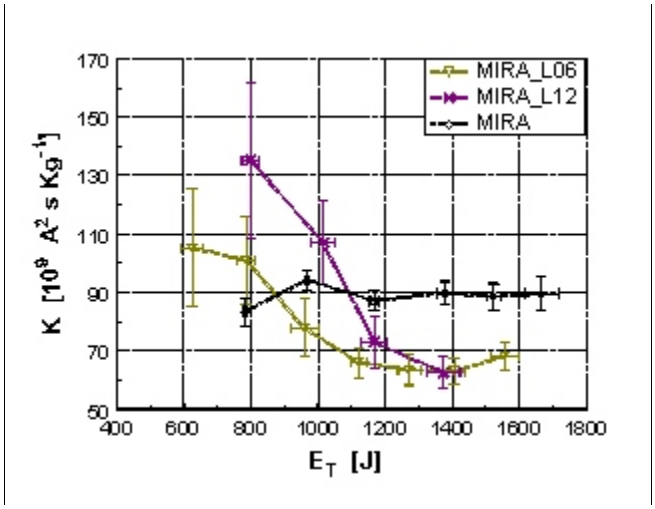

Figure 9 - The self-applied magnetic field changes the behavior of the K parameter as a function of energy, E_T.

With energy, E_T, kept constant, at the lower energies, MIRA_L12 shows the highest values. On increasing the energy, the difference between MIRA_L06 and MIRA_L12 decreases, until, at the highest energies, the differnce becomes negligible. Moreover at such energies, the baseline MIRA shows the highest values.

Jet Exhaust Velocity

The axial ion velocity, shows a general trend towards decreasing velocity as both E_T and Ψ increase (see Fig. 10). At constant Ψ, MIRA_L06 exhibits the lower velocity.

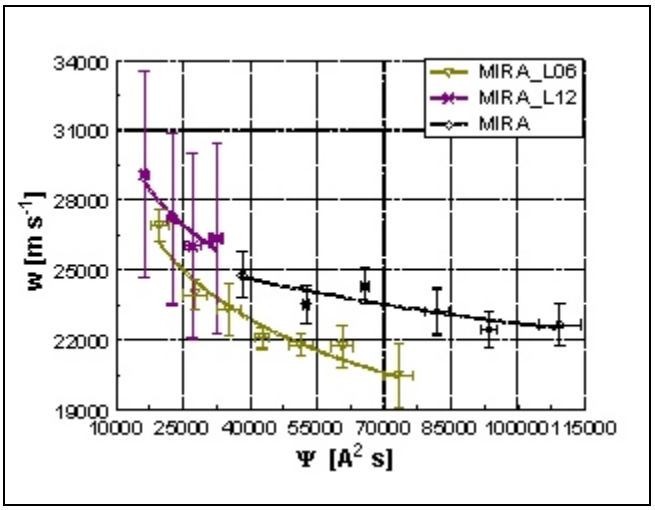

Figure 10 - Ion exhaust velocity shows substantial data scatter and a tendency to decrease with increasing Ψ.

Impulse Bit

Impulse bit increases linearly as a function of both energy, E_T, and current parameter Ψ (Figs. 11, 12). A comparison of the thruster systems at constant energy shows:

$$(I_b)_{MIRA} > (I_b)_{MIRA\_L06} > (I_b)_{MIRA\_L12} .$$

At constant current parameter, Ψ, the opposite holds.

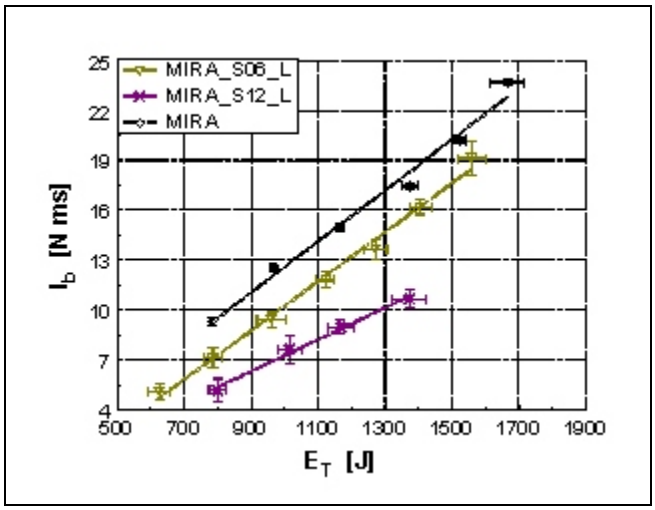

Figure 11 - Linear behavior of impulse bit, I_b, as a function of energy E_T .

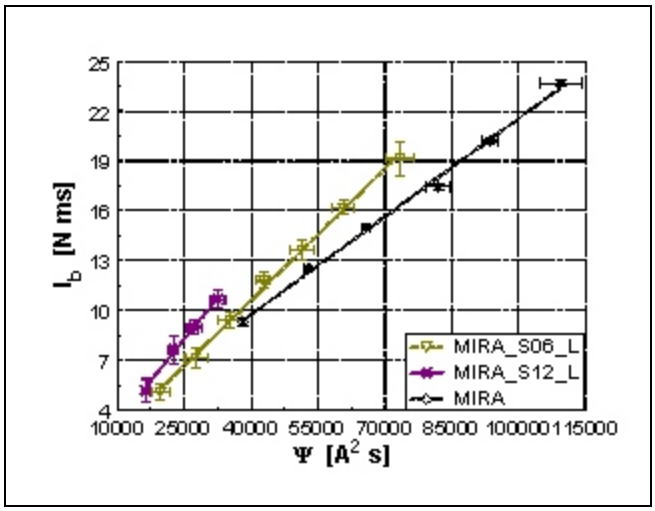

Figure 12 - Linear behavior of impulse bit, I_b, as a function of current parameter, Ψ .

Thrust Efficiency

The thrust efficiency can be written

$$\eta = \frac{I_b^2}{2\,m\,E_T}. \qquad (8)$$

It appears to be widely scattered (Fig. 13). The baseline MIRA and the MIRA_L06 show similar characteristics but at different power levels, while the MIRA_L12 thruster exhibits decreasing values, with increasing currents.

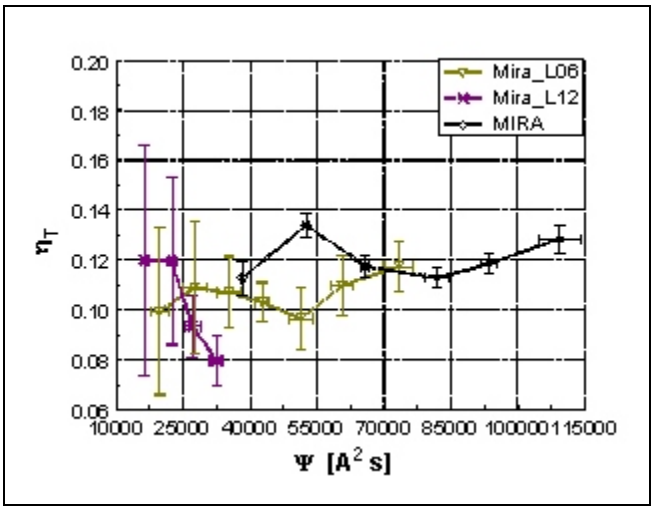

Figure 13 - Thrust efficiency significant data scatter as a function of current parameter.

Discussion

Previous studies[16,18,19] have shown that the magnetic field due to the coil feeding conductors is negligible. Based on the coil length, the self-applied magnetic field inside the acceleration duct can be considered as an almost purely axial field, i.e. $\underline{\mathbf{B}} \approx \underline{\mathbf{B}}_z$ (see Fig.1).

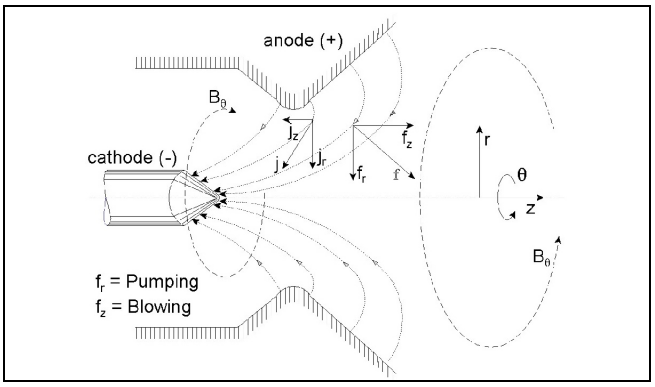

Figure 14 - The discharge components.

The volume force acting on the plasma inside the acceleration duct can be written:

$$\underline{\boldsymbol{f}} = \underline{\boldsymbol{J}} \times \underline{\boldsymbol{B}} = \\ = (J_r \hat{r} + J_z \hat{z}) \times (B_\theta \hat{\theta} + B_z \hat{z}), \qquad (9)$$

where J_z and J_r are the components of the discharge (see Fig. 14), and B_θ is the component of the magnetic field self-induced by the discharge. This force can be seen as

the sum of the two terms:

$$\underline{f} = (J_r \hat{r} + J_z \hat{z}) \times B_\theta \hat{\theta} + \\ + (J_r \hat{r} + J_z \hat{z}) \times B_z \hat{z} = \\ = (J_r \hat{r} + J_z \hat{z}) \times B_\theta \hat{\theta} + (J_r \hat{r} \times B_z \hat{z}) , \quad (10)$$

The first is due to the discharge alone and leads to the Maecker's law[9,10] (2). The second is due to the presence of the coil and results in an azimuthal volume force,

$$\underline{f_{B_z}} = - J_r \hat{r} \times B_z \hat{z} = J_r B_z \hat{\theta} , \quad (11)$$

that poses the plasma in a positive rotation.

Based on the generalized Ohm's law

$$\underline{J} = \sigma (\underline{E} + \underline{u} \times \underline{B}) - \frac{\Omega}{B} (\underline{J} \times \underline{B}) , \quad (12)$$

an azimuthal component of the current density is generated inside the acceleration duct

$$j_\theta = \sigma \left(E_\theta + u_z B_r - u_r B_z \right) + \\ - \frac{\Omega}{B} \left(j_z B_r - j_r B_z \right) . \quad (13)$$

Since, based on the initial assumption, the radial component of the magnetic field can be neglected [see (8)], and since, following the previous treatments[9] leading to the Maecker law, E_θ and u_r can also be neglected, the azimuthal current reduces to

$$j_\theta = - \frac{\Omega}{B} j_r B_z . \quad (14)$$

The latter interact again with the axial component of the magnetic field, resulting in a radial volume force:

$$\underline{f_{J_\theta}} = J_\theta \hat{\theta} \times B_z \hat{z} = J_\theta B_z \hat{r} . \quad (15)$$

This force acts only in the region of space where the radial component of the discharge is also present and, based on the cited treatment of MPD thrust, enhances the "pumping" effect, i.e. augments the overall thrust[9,18].

It should be noted that the azimuthal component of the current induces a magnetic field that opposes that created by the coil, reducing the overall effect of the self-applied magnetic field.

In the previous treatments, the theoretical thrust, due to the self-induced magnetic field, has been calculated by taking into account only the forces acting inside the space occupied by the discharge; these treatments lead to a perfectly axial exhaust velocity[9]. Actually the arc geometry involve the presence of a radial component of the velocity, that has been neglected. Then the plasma downstream the region of space occupied by the discharge has two main component of velocity:

$$\underline{w} = w_z \hat{z} + w_\theta \hat{\theta} , \quad (16)$$

and travels in a region of space where the self-applied magnetic field and an azimuthal self-induced magnetic field due only to the radial component of the discharge[8] are present:

$$\underline{B} = B_z \hat{z} + B_r \hat{r} + B_\theta \hat{\theta} . \quad (17)$$

Therefore, the Lorentz force acting on the plasma downstream the discharge can be written as:

$$\underline{f} = q \, \underline{w} \times \underline{B} = \\ = q \, [(w_\theta B_z - w_z B_\theta) \hat{r} + w_z B_r \hat{\theta} - w_\theta B_r \hat{z}] . \quad (18)$$

The effect of the Lorentz force is, hence, to diminish the axial velocity of the plasma while augmenting the azimuthal velocity, so reducing the overall thrust.

The radial component of the force causes a radial speed; then the Lorentz force becomes:

$$\underline{f} = q \, \underline{w} \times \underline{B} = \\ = q \, [(w_\theta B_z - w_z B_\theta) \hat{r} \\ + (w_z B_r - w_r B_z) \hat{\theta} + (w_r B_\theta - w_\theta B_r) \hat{z}] . \quad (19)$$

If the radial force component is negative ($w_\theta B_z < w_z B_\theta$) it generates a negative radial velocity; as a consequence, the azimuthal force component is positive and the axial component is negative. Hence the axial component of the

velocity decreases while the azimuthal component increases until the radial component of the force becomes positive ($w_\theta B_z > w_z B_\theta$). If the radial component of the velocity is positive and large enough that $w_r B_\theta > w_\theta B_r$ the opposite is true.

This force acts so that the radial component of the plasma velocity oscillates between negative and positive values. In other words, the plasma starts expanding and contracting, while experiencing axial acceleration and deceleration respectively.

The thrust is due to the "final" axial velocity of the plasma i.e. to the velocity of the plasma no longer subject to the Lorentz force. This occurs in the two following cases:

- the plasma, moving away from the thruster, moves through a magnetic field which becomes progressively weaker; since the Lorentz force does no work on the plasma, the speed holds constant, even if components of the velocity change; such speed, sooner or later, equals the local Alfven speed and the plasma is then no longer influenced by the magnetic field[22];
- the discharge expires and the magnetic field disappears.

Electrical Parameters

At constant Ψ, the difference between the impedances of MIRA_L12 and MIRA_L06_L is much bigger than the one between the impedances of MIRA_L06 and MIRA. This is consistent with the higher axial magnetic field generated by the twelve-turn coil. In fact, at equal currents, the strongest the axial magnetic field, the biggest the potential difference necessary to bring the electrons from the cathode to the anode. Therefore the total impedance of the discharge path increases.

Ablated Mass

The higher ablated mass of the thrusters with the coil, at constant Ψ, is due to the swirl generated by the self-applied magnetic field: the azimuthal current and the hot plasma, hitting the propellant bars, ablate more material. The presence of the swirl in the propellant zone is confirmed by experimental evidence[16-19]: in the thrusters with a self-applied magnetic field, more remarkable traces of propellant deposition were found on the sides of the propellant bars hit by the swirling plasma.

Jet Exhaust Velocity

The characteristics of the exhaust velocity are consistent with the *K* parameter. In particular, the highest velocity values of MIRA_L12, compared to MIRA_L06, point to the smaller divergence of the exhaust plume, due, once more, to the higher self-applied magnetic field.

Impulse Bit

The experimental results show (Fig. 12) that, at equal Ψ, the positive thrust contribution due to the (14) component is bigger than the negative contributions of the other components [see (17)]. This effect increases as the magnetic field increases.

The higher impedances, i.e. the higher energy losses, justify the impulse bit, I_b, decrease as the self-applied magnetic field increases, at constant energy, E_T. In that these losses are due to the coil impedance, the employment of superconductor wires could be a solution to be considered, in particular in the high power propulsive systems.

Summary and Conclusions

Solid propellant MPD thruster behavior was examined with self-applied magnetic fields of different intensities. Two thrusters with respectively a six-turn and a twelve-turn coil surrounding 7/9 of the same chamber-anode-nozzle were tested along with the baseline thruster. The same current which creates the discharge, also flows through the coils. All thrusters used coaxial electrodes with six radially-mounted Teflon® propellant bars surrounding the cathode tip. Measurements included electrical characteristics, impulse bit (thrust stand),

exhaust velocity (TOF Langmuir probe system), and ablated propellant mass per shot.

The focus of the test program was to evaluate the effect of the self-applied magnetic field on the thruster performance as functions of E_T and Ψ: The linearly dependent behavior of E_T and Ψ was also confirmed for this type of thrusters.

At constant Ψ, higher self-applied magnetic fields lead to higher impedances, higher ablated mass, and, most importantly, higher impulse bit. The latter is due to the the additional "pumping" effect caused by the interaction between the discharge and the axial external magnetic field inside the acceleration duct. The positive effect of this is larger than the negative effect due to the interaction between the external magnetic field and the plasma exhaust flow in the remaining part of the acceleration region (outside the discharge region).

On the other hand at constant energy, E_T, the thrust gained by applying the magnetic field does not justify the energy lost to feed the coil. A remedy to this problem could be to use a coil with superconductor wires.

Acknowledgments

We would like to thank C. Chingari for the precision with which he fabricated all of the thruster components.

The funding provided by the Italian Space Agency (ASI) and the Italian Ministry of Research (MURST) is gratefully acknowledged.

References

[1] Paccani G., Petrucci L. and Deininger W. D., "Scale Effects On Solid Propellant MPD Thruster Performance", *AIAA Paper 98-3473, 34th JPC, Cleveland, Ohio (USA),* July 1998.

[2] Paccani G., "A Coaxial Non-Steady Solid Propellant MPD Thruster Experimental Analysis", *IEPC Paper 87-1095. 19th IEPC, Colorado Springs, Colorado (USA),*May 1987. - *Journal of the British Interplanetary Society Vol. 41, pp. 253-240,* 1988.

[3] Paccani G., "Experimental Analysis of a Coaxial Solid Propellant MPD Thruster with Segmented Anodes", *IEPC Paper 93-159, 23rd IEPC, Seattle, Washinghton (USA),* September 1993.

[4] Paccani G., Chiarotti U. and Deininger W. D., "Quasi-Steady Ablative Magneto-plasmadynamic Thruster Performance with Different Propellants", *Journal of Propulsion and Power, Vol..14, No. 2, pp. 254-260.* March-April 1998.

[5] Paccani G., "Non-Steady Solid Propellant MPD Thruster Experimental Analysis Concepts", *IEPC Paper 90-2674, 21st IEPC, Orlando, Florida (USA)*, July 1990.

[6] Paccani G., "Studi sui Meccanismi Fisici di Base nei Propulsori MPD"; *ASI 92-RS-27 Report n 1,* April 1993 (In Italian).

[7] Paccani G.: "Anode-Nozzle Experimental Analysis in a Coaxial non Steady Solid Propellant MPD Thruster", *IEPC Paper 88-076, 20th IEPC, Garmisch-Partenkirchen, Germany,* October 1988.

[8] Paccani G., Petrucci L. and Deininger W. D., "Experimental Analysis of a Solid Propellant MPD Thruster with Different Anode Radii", *IEPC Paper 99-235, 26th IEPC., Kitakyushu, Japan,* October 1999.

[9] Jahn G. R., "*Physics of Electric Propulsion*", New York: Mc Graw Hill, 1968.

[10] Maecker H., "Plasmastromungen in Licht-bogen infolge eigenmagnetischer Kompression", *Zeitschrift für Physik, Bd. 141, pp. 198-216,* 1955 (in German).

[11] Krülle G. and Zeyfang E., "Preliminary Conclusions of Continuous Applied Field Electromagnetic Thruster Research at DFVLR", *AIAA paper 75-417, 11th IEPC, New Orleans, Louisiana (USA),* March 19-21, 1975.

[12] Tahara H., Sasaki M., Kagaya Y. and Yoshikawa T., "Thruster Performance and Acceleration Mechanisms of a Quasi-steady Applied Field MPD Arcjet", *AIAA Paper 90-2554, 21st IEPC, Orlando, Florida (USA),* July 18-20, 1990.

[13] Sasoh A., "Thrust Formula for an Applied-Field MPD Thruster Derived from Energy Conservation Equation". *IEPC Paper 91-062, 22nd IEPC, Viareggio, Italy,* October 14-17, 1991.

[14] Lawless J. L. and Subramaniam V. V., "A Review of the Theory of Self-Field MPD Thrusters", *IEPC Paper 91-019, 22nd IEPC, Viareggio, Italy,* October 14-17, 1991.

[15] Sasoh A. and Arakawa Y.: "Electromagnetic Effects in an Applied-Field Magnetoplasmadynamic Thruster", *Journal of Propulsion and Power, Vol. 8, No. 1,* January 1992.

[16] Paccani G.: "Solid-propellant Quasi-steady Mpd Thrusters with Self-Applied Magnetic Field", *32nd JPC, Lake Buena Vista, FL (USA),* July 1-3, 1996.

[17] Paccani G. and Petrucci L., "Self-Applied Magnetic Field Effects On Solid Propellant MPD Thruster Performance", *IEPC Paper 01-140, 27th IEPC, Pasadena, California (USA),* October 2001.

[18] Fiori L., "Propulsori MPD con Campo Magnetico Autoapplicato", *LAUREA Thesis in Ingegneria Aeronautica, Università degli Studi di Roma "La Sapienza",* a.a. 1996-1997 (In Italian).

[19] Ralli C., "Analisi Sperimentale del Campo Magnetico in Propulsori MPD", *LAUREA Thesis in Ingegneria Aeronautica, Università degli Studi di Roma "La Sapienza",* a.a. 1997-1998 (In Italian).

[20] Paccani G. and Ravignani R., "Sistema per la misura della spinta di propulsori MPD", *Aerotecnica, Missili e Spazio, Vol. 72, pp. 42-51, No. 1,* Jan-Jun 1994 (In Italian).

[21] Paccani G. and Di Zenzo S., "Computerized Jet Velocity Measurements in MPD Thrusters", *Aerotecnica, Missili e Spazio, vol 74, No. 3-4, pp. 93-102,* Jul-Dec 1995.

[22] Chang Diaz F., Squire J., Bengston R., Breizman B., Baity F. and Carter M., "The Physics and Engineering of the VASIMR Engine", *AIAA Paper 00-3756, 36th JPC, Huntsville, Alabama (USA),* July 2000.